European Journal of Pharmaceutics and Biopharmaceutics 76 (2010) 83–94

Contents lists available at ScienceDirect

European Journal of Pharmaceutics and Biopharmaceutics

journal homepage: www.elsevier.com/locate/ejpb

Research paper

Mechanism-based prediction of particle size-dependent dissolution and absorption: Cilostazol pharmacokinetics in dogs

Stefan Willmann [a,*], Kirstin Thelen [a,b], Corina Becker [a], Jennifer B. Dressman [b], Jörg Lippert [a]

[a] Bayer Technology Services GmbH, Competence Center Systems Biology and Computational Solutions, Leverkusen, Germany
[b] J.-W. Goethe University, Institute of Pharmaceutical Technology, Frankfurt a.M., Germany

ARTICLE INFO

Article history:
Received 3 November 2009
Accepted in revised form 2 June 2010
Available online 8 June 2010

Keywords:
Modeling
Simulation
Dissolution
Particle size
Absorption
IVIVC

ABSTRACT

A previously developed physiologically based pharmacokinetic (PBPK) model for gastro-intestinal transit and absorption was combined with a mechanistic dissolution model of the Noyes–Whitney type for spherical particles with a predefined particle size distribution. To validate the combined model, the plasma concentration–time curves for cilostazol obtained in beagle dogs using three different types of suspensions with varying particle diameters were simulated. *In vitro* dissolution information was also available for different formulations, but this data could only predict the *in vivo* outcome qualitatively. The mechanistic PBPK model, on the other hand, could predict the influence of the particle size on the rate and extent of absorption under both fasted and fed conditions accurately, and the gap between the *in vitro* dissolution data and the *in vivo* outcome could successfully be explained.

We conclude that by integrating the processes of particle dissolution, gastro-intestinal transit and permeation across the intestinal epithelium into a mechanistic model, oral drug absorption from suspensions can be predicted quantitatively. The model can be applied readily to typical formulation development data packages to better understand the relative importance of dissolution and permeability and pave the way for successful formulation of solid dosage forms.

1. Introduction

The rate and extent of oral drug absorption *in vivo* are two key properties that decide the success of a drug development candidate. It is well known that a number of factors influence drug absorption from the gastro-intestinal (GI) tract after administration as a solid oral dosage form. The complex interplay between the events of drug release, dissolution, permeation across the intestinal epithelium, and pre-systemic metabolism in the gut wall and liver ultimately determines the rate and extent of systemic availability.

In the pharmaceutical industry, dissolution testing is widely used for development and quality control of oral formulations. Standardized *in vitro* dissolution test methods have been established to characterize the rate and extent of the drug release and dissolution from oral solid dosage forms. In combination with biorelevant dissolution media such as fasted (FaSSIF) or fed state simulated intestinal fluid (FeSSIF), these tests can be used to predict the *in vivo* dissolution behavior of orally administered dosage forms [1–4].

The quantitative relationship between *in vitro* dissolution data and *in vivo* pharmacokinetic data is often referred to as "*in vitro–in vivo* correlation" (IVIVC). IVIVC allows effective dosage form optimization with the fewest possible trials in man, allows definition of dissolution acceptance criteria, and can be used as a surrogate for further bioequivalence studies; it is also recommended by regulatory authorities [5–9]. Another systematic approach to link *in vitro* dissolution with *in vivo* bioavailability combines dissolution behavior with the solubility and permeability characteristics of the drug; this is the Biopharmaceutics Classification System (BCS) [10]. For certain classes of drugs that can meet the BCS criteria, bioequivalence may be established based solely on the *in vitro* dissolution, i.e. by waiving *in vivo* studies in humans ("Biowaiver") [11–13]. A third approach, physiologically based absorption modeling, has also recently been applied to support justification of the biowaiver by quantitatively combining experimentally obtained biorelevant solubility, intestinal permeability, and dissolution profiles [14–18]. Several physiologically based models for GI transit and absorption have been developed. These aim towards a prediction of the *in vivo* oral drug absorption from a combination of a set of physiological properties such as dimensions and transit times of the GI tract as well as a set of physicochemical parameters/*in vitro* properties of the substance [19,20]. Some of these models have become available in the form of commercial software tools such as GastroPlus™ and PK-Sim® [21,22].

* Corresponding author. Address: Bayer Technology Services GmbH, BTS-PT-AS-Systems Biology and Computational Solutions, Building E41, D-51368 Leverkusen, Germany. Tel.: +49 214 30 36568; fax: +49 214 30 50698.
E-mail address: stefan.willmann@bayertechnology.com (S. Willmann).

0939-6411/$ - see front matter © 2010 Elsevier B.V. All rights reserved.
doi:10.1016/j.ejpb.2010.06.003

In this study, we report the development of a mechanistic model that simulates the dissolution of a solid dosage form during GI transit under physiological conditions. For the evaluation of the model, cilostazol, a BCS class II (low solubility–high permeability) synthetic platelet inhibitor, was chosen because the dissolution and absorption behavior of this drug has been intensively studied by Jinno et al. *in vitro* and *in vivo* [23]. The authors measured the plasma kinetics of cilostazol after the administration of three different suspensions containing cilostazol with varying particle size distributions under fasted and fed conditions in beagle dogs. In addition, the *in vitro* dissolution profiles of the three types of suspensions were reported in both water and biorelevant dissolution media. Although the *in vitro* dissolution profiles showed an influence of particle size, the data were not able to quantitatively predict either the increase in bioavailability with decreasing particle size or the food effect observed *in vivo* [23]. The aim of this work was to demonstrate that the gap between the *in vitro* dissolution tests and the *in vivo* PK behavior can efficiently be bridged with the help of mechanistic, physiologically based pharmacokinetic simulations.

2. Methods

2.1. PBPK model for gastro-intestinal transit and absorption in beagle dogs

The details of the generic, physiologically based GI transit and absorption model used in this study have been published in detail for rats [24], monkeys [25], and humans [26]. In short, the intestinal lumen in this model is described as a tube with spatially varying properties, e.g. the effective surface area that is available for absorption and the pH value. Drug flow through the intestinal lumen is modeled using a continuous transit function, which is approximated by a Gauss profile of oscillating width with a continuously moving center of mass of the drug package. Scaling between different species is achieved by using species-specific physiological model input parameters (dimensions of the intestinal segments, effective surface area, regional pH values, gastric emptying time (GET), and small intestinal transit time (SITT)) as discussed in detail in the above-mentioned papers [24–26]. The relevant physiological parameters of the GI tract of beagle dogs have been collected from the literature and are summarized in Table 1.

The small intestine of a beagle dog is about 280–300 cm in length in the flaccid state [27–29]. However, the small intestinal length in the living animal appears to be considerably shorter [30,31]. In the model, the small intestine is described as a tube with a total length L_{SI} of 200 cm [31] and a constant radius of 0.5 cm along the entire small intestine [27,29]. The small bowel is divided into three segments, representing the duodenum (first 25 cm), the jejunum (length 167 cm), and the ileum (last 8 cm) [27]. The effective surface area available for absorption can be calculated based on the geometric area of the tube and the surface amplification due to villi and microvilli [26,30]. The height and radius of the villi in beagle duodenum, jejunum, and ileum, respectively, have been reported by Kuzmuk et al. [32], and their density is given by Taylor and Anderson [33]. For the amplification factor of the microvilli in dog small intestine, a mean value of 25 was used [33,34]. Since the beagle is a carnivorous species, there is a little need for fermentation in the GI tract. As a result, the large intestine is short, essentially consisting of a hollow tube without sacculations. The (poorly developed) caecum is 4–6 cm in length and 1.5–2 cm in diameter [27]. The colon of dogs is about 25 cm long and measures about 2 cm in diameter throughout its length. The rectum is straight, about 5 cm long and 3 cm in diameter [27,30].

Table 1
Physiological parameters of the gastro-intestinal tract in adult beagle dogs (for details and references, see text).

Parameter	Value
Length (cm)	
–Duodenum	25
–Jejunum	167
–Ileum	8
–Total small intestine	200
Radius (cm)	
–Duodenum	0.50
–Jejunum	0.50
–Ileum	0.50
Luminal Volume SI (mL)	160
Effective Surface Area SI (cm^2)	1.44×10^5
pH value stomach (fasted/fed)	1.5/2.1
pH values SI/caecum (fasted, fed)	
–Duodenum	6.2
–Upper jejunum	6.2
–Lower jejunum	6.6
–Upper ileum	7.5
–Lower ileum	7.5
–Caecum	6.4
GET (fasted, first order process)	0.5 h
GET (fed, zero order process)	1.5 h
SITT (fasted)	4.5 h
SITT (fed)	5.0 h

In the PBPK model, GET τ_{GE} is defined as the time when the remaining volume equals $1/e \sim 36.8\%$ of the initial volume under fasted conditions, and as the time of complete gastric emptying (GE) under fed conditions. It appears that GE of liquids is quantitatively similar in dogs and humans in the fasted state, whereas emptying in the postprandial state may take considerably longer in dogs than in humans [35]. Using the absorption time of acetaminophen in solution as a marker for GET, the physiological elimination half-life of liquid from the stomach of fasted dogs ranged from a few minutes to values exceeding half an hour [36–41]. Mean emptying time of radio-opaque particles of 1 mm in diameter was about half an hour in fasted beagles [42]. By contrast, complete emptying of a barium sulfate suspension from the stomach into the small intestine of fasted beagles was reported to take almost 76 min (SD ± 16.7 min) [43]. However, the high density of the marker and the fact that the radiographs were made at comparatively long (30-min) intervals may have influenced the results. Based on the reported values, a mean GET of 30 min was set for τ_{GE} in fasted beagles.

The effect of meals on GE of an acetaminophen suspension has been assessed in 12 beagle dogs [44]. The mean absorption time of acetaminophen was clearly prolonged after ingestion of a meal in proportion to the size of the meal (mean values ~0.3 h in the fasted state and ~0.4, ~0.8, and about 2 h for the 50 g, 100 g, and 300 g meal, respectively) [44]. Furthermore, GET was affected by the composition of the meal [44,45]. In the study of Itoh and coworkers [42], the mean emptying time of the smallest (1 mm) radio-opaque particles was about 1.8 h after consumption of 50 g of dog food. An overview of the different studies on GE in dogs fed with different types of liquids or meals is given in [45]. Reported GE half-times range from 10 min for water to several hours for dry kibble food. It should be noted that for smaller meal sizes, liquid is emptied faster than the solid fraction of the meal [35].

Jinno et al. [23] fed their beagles 170 g of a solid food containing 24% protein and 9% fat (635 kcal) 30 min prior to dosing of cilostazol. Based on the GET reported in the literature and in consideration of the size and composition of the meal administered in the *in vivo* study, a default value of $\tau_{GE} = 90$ min appears to be a reasonable estimate to simulate fed state pharmacokinetics of cilostazol suspensions in the Jinno study.

The transit time through the small intestine represents another important physiological parameter determining drug absorption. In the majority of cases, the values reported for SITT in beagles refer to the first appearance of an orally administered marker in the caecum, whereas in the PBPK model, the SITT t_{SI} is defined as the time at which 90% of the administered marker has reached the caecum [24]. Using the first appearance of sulfapyridine, a bacterial metabolite of salicylazosulfapyridine in colon, in plasma as marker for GI transit, mean oro-caecal transit time in fasted beagles ranged between 2.0 ± 1.1 h and 5.67 ± 2.52 h (mean and SD) in a number of studies [36–40]. Using barium sulfate as a marker, mean SITT of the head of the contrast medium column was only 73 ± 16.4 min [43]. The majority of contrast medium emptied from the small intestine into the caecum within about 4 h (mean and SD 214 ± 25.1 min).

In the fed state, small intestinal transit patterns appear to be independent of the size of the meal, although it has been suggested that ingestion of a high-fat meal causes a delay in SITT [44]. In a similar study, no differences in the rate of transit among different particle sizes were observed [45]. Based on the above-mentioned values, a mean SITT for the bulk of material (90%) of about 4–5 h appears to be reasonable. The comparatively small amount of fat of the meal given in the study of Jinno and co-workers (see above) was assumed to have only a minor effect on SITT.

Although the pH of the gastro-intestinal contents can be assumed to have no effect on the solubility of neutral molecules such as cilostazol, future application of the generic beagle model to acids and bases where luminal solubility will depend on the pH value in the respective segment is planned. For this purpose, the pH profile along the GI tract of the beagle has been implemented into the model database underlying PBPK models in PK-Sim® [35,46–48]. The data in Table 1 do not reflect the existence of fluctuations in gastric pH, which have been observed in fasted beagles [42].

2.2. PBPK model for distribution in the body

In addition to the parameters of the GI tract described above, further physiological information such as volumes and blood flow rates of the organs is required to simulate the post-absorptive drug distribution. This information has also been collected from the literature and is summarized in Table 2. Most organ volumes (assuming a density of 1 g/mL) of a mean male beagle dog weighing 10.5 kg were taken from [27]. The volumes of the skin and adipose tissue in beagle dogs could have not been reported in the literature. With a body surface area of about 0.5 m^2 [49,50] and a thickness of the epidermis and dermis of 27 μm and 1.027 mm, respectively [27], the volume of the skin of the beagle dog is calculated to account for 4.8% of body weight and is quite similar to the value suggested for smaller dogs (4.3%) [51]. The subcutis was treated as adipose tissue. The reported total blood volume (82 mL/kg body weight in the beagle [27]) was allocated to the various organs according to their fractional volume of vascular space [51] and to the three major blood "pools", namely the portal vein, the arterial blood, and the venous blood pool. The contribution of the portal vein volume had to be scaled from other species already implemented in the software tool (human, rat, and mouse). Finally, the adipose tissue was used to make up the difference in body weight after all other weights were set. This resulted in an adipose volume of 20% of total body weight, close to the value of ~18% previously suggested for smaller dogs [51].

In beagle dogs weighing 8–12 kg, cardiac output values are 900–2700 mL/min under anaesthesia and somewhat higher (1300–3000 mL/min) in the standing position [27]. Mean cardiac output was estimated to be about 2000 mL/min and was distributed over the various organs and tissues based on literature data (see Table 2) [27,51–54].

Table 2
Physiological parameters of the beagle (BW 10.5 kg) relevant for PBPK modeling.

Tissue	Organ volume (mL)	Organ blood flow (mL/min)
Bone	880	172
Brain	73	51
Adipose	2101	65
Gonads (Testes)	10	2
Heart	81	103
Kidneys	50	346
Stomach	85	53
Small intestine	266	232
Large intestine	61	69
Liver	373	102
Lung	68	1915
Muscle	5387	457
Pancreas	22	39
Skin	500	154
Spleen	27	72
Portal vein	150	464

2.3. Model for particle size-dependent dissolution

The mathematical background of the mechanistic model for dissolution of spherical particles with a predefined particle size distribution was adopted from Johnson [55]. Fig. 1 shows a schematic representation of the dissolution model.

The total amount of solid drug that is administered (X_o) is split into k particle size groups. Each group contains a given number of particles (N_i) that remains constant over time (defined by the particle size distribution). The initial amount of drug in each particle size group ($X_{o,i}$) is then given by

$$X_{o,i} = N_i \rho \frac{4}{3}\pi r_{o,i}^3, \quad i \in [1 \ldots k] \left(\text{with } \sum_{i=1}^{k} X_{0,i} \stackrel{!}{=} X_0 \right) \tag{1}$$

where ρ denotes the density of the drug material, and $r_{o,i}$ denotes the initial radius of the ith particle size group. Upon administration, the drug material is assumed to disintegrate and to start its passage through the GI tract. The transit through the GI tract is modeled using an empirical transit function that defines the fraction of the administered dose that is located at position z at time t after administration [24]. The dissolution process is described by a differential equation of the Noyes–Whitney type. The local kinetics of the amount of solid ($X_{\text{solid},i}$) and dissolved ($X_{\text{dissolved},i}$) drug material are given by [55]:

$$\frac{dX_{\text{solid},i}(z,t)}{dt} = -\zeta_i X_{0,i}^{1/3} X_{\text{solid},i}^{2/3}(z,t)(S_{\text{int}}(z) - C_{\text{lumen}}(z,t)) \quad \text{and}$$
$$\frac{dX_{\text{dissolved},i}(z,t)}{dt} = \zeta_i X_{0,i}^{1/3} X_{\text{solid},i}^{2/3}(z,t)(S_{\text{int}}(z) - C_{\text{lumen}}(z,t)), i \in [1..k] \tag{2}$$

with

$$\zeta_i = \frac{3D}{\rho h r_{0,i}}, \quad i \in [1..k] \tag{3}$$

In these equations, ζ_i denotes a dissolution parameter that is constant for a given group of particles with radius $r_{o,i}$, D is the aqueous diffusion coefficient of the drug, h the thickness of the diffusion layer [55]. $S_{\text{int}}(z)$ is the solubility of the drug in the intestinal fluid at position z, and C_{lumen} the luminal concentration of the dissolved drug. Note that the drug amounts X as well as C_{lumen} are a function of time and the spatial coordinate in the intestinal tract, and the solubility can vary with the local pH in the intestinal lumen [24,26]. $C_{\text{lumen}}(z,t)$ is calculated as the total amount of drug

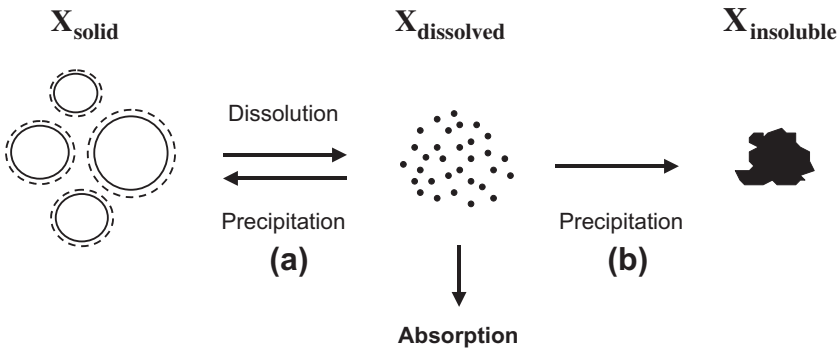

Fig. 1. Structure of the dissolution model: solid spherical particles of different diameters can be dissolved in the intestinal lumen. Precipitation can occur leading either to an increase in the administered solid form (a) or to a new entity of the drug, which is treated as insoluble (b). The fraction dissolved at any time in the gut lumen is available for absorption in the combined dissolution and absorption model.

(i.e. summarized over all particle size groups) that is dissolved within a given cylindrical volume element of the small intestine (with local radius R_{SI}):

$$C_{\text{lumen}}(z,t) = \frac{dX_{\text{dissolved}}(z,t)}{\pi R_{SI}^2(z)dz} \quad \text{with}$$

$$dX_{\text{dissolved}}(z,t) = \sum_{i=1}^{k} dX_{\text{dissolved},i}(z,t) \tag{4}$$

This concentration is the driving force for passive diffusion across the intestinal epithelium. The amount of drug that permeates across the intestinal membrane and is subsequently absorbed (X_{absorbed}) at position $[z\ldots z+dz]$ in a time interval $[t\ldots t+dt]$ is calculated as [24,26]:

$$\frac{d^2X_{\text{absorbed}}(z,t)}{dzdt} = P_{\text{int}}\left[C_{\text{lumen}}(z,t) - \frac{C_{PV}(t)}{K_{\text{lumen}}}\right]\frac{dA_{eff}}{dz} \tag{5}$$

Here, P_{int} denotes the intestinal permeability coefficient, $C_{PV}(t)$ is the drug concentration in the portal vein, K_{lumen} represents the equilibrium partition coefficient between the portal blood and the luminal content, and dA_{eff} is the effective surface area that is available for absorption in the intestinal region $[z\ldots z+dz]$. The latter is calculated using the information about regional dimensions as surface amplification factors as described in Section 2.1 (see also Table 1). After absorption into the portal vein, the absorbed amount of drug is transported to the liver and – if not subject to first pass elimination – becomes available for systemic distribution within the PBPK model.

If sink conditions ($C_{\text{lumen}} \gg C_{PV}$, i.e., $K_{\text{lumen}} \to \infty$) can be assumed, Eq. (5) reduces to:

$$\frac{d^2X_{\text{absorbed}}(z,t)}{dzdt} = P_{\text{int}}C_{\text{lumen}}(z,t)\frac{dA_{eff}}{dz} \tag{6}$$

As can be seen in Eq. (2), dissolution occurs whenever the local luminal concentration is lower than the intestinal solubility. As a consequence of dissolution, the size of each particle is reduced. As the particle size approaches the dimension of a single drug molecule, the description of a continuous drug mass in Eq. (2) becomes meaningless. Therefore, a threshold for a minimal relevant particle radius ($r_{\min}$) needs to be defined in the model. If the particle radius falls below this limit ($r_i < r_{\min}$), the remaining drug mass is assumed to dissolve instantaneously in the subsequent time step.

If the luminal concentration exceeds the intestinal solubility, e.g. as a result of a pH-induced solubility decrease in case of bases moving down the GI tract or as a result of a decrease in the available volume of intestinal fluids, the drug may precipitate in the intestinal lumen [55]. For the PBPK model, two alternative precipitation scenarios were considered: The first scenario, indicated by the arrow marked (a) in Fig. 1, is simply the inverse of the dissolution process, i.e., the precipitated drug amount is added to the solid drug mass, leading to in increase of the particle size. In the second scenario, the precipitated drug amount is assumed to be insoluble ($X_{\text{insoluble},i}$; indicated by the arrow marked (b) in Fig. 1). The precipitated drug amount is removed from the dynamic system in this scenario and Eq. (2) is replaced by the following set of equations (in case of $C_{\text{lumen}} > S_{\text{int}}$):

$$\begin{aligned} &\frac{dX_{\text{solid},i}}{dt} = 0, \frac{dX_{\text{dissolved},i}}{dt} = \zeta_i X_{0,i}^{1/3} X_{\text{solid},i}^{2/3}(S_{\text{int}} - C_{\text{lumen}}) \\ &\frac{dX_{\text{insoluble},i}}{dt} = -\zeta_i X_{0,i}^{1/3} X_{solid,i}^{2/3}(S_{\text{int}} - C_{\text{lumen}}), \quad i \in [1\ldots k] \end{aligned} \tag{7}$$

The difference to Eq. (3) is that here the precipitated amount of the dose forms a new species ("insoluble"), while the original form of the drug ("solid") remains constant during precipitation.

As model output, the fractions (F) of the different drug species relative to the total drug amount are calculated as a function of time:

$$\left.\begin{aligned} F_{\text{solid}}(t) &= X_{\text{solid}}(t)/X_0 \\ F_{\text{dissolved}}(t) &= X_{\text{dissolved}}(t)/X_0 \\ F_{\text{insoluble}}(t) &= X_{\text{insoluble}}(t)/X_0 \end{aligned}\right\} \tag{8}$$

Here X_{solid}, $X_{\text{dissolved}}$, and $X_{\text{insoluble}}$ denote the total amounts of solid, dissolved, and insoluble drug in the GI tract, which are obtained from:

$$X_{\text{solid}} = \sum_{i=1}^{k} X_{\text{solid},i}, X_{\text{dissolved}} = \sum_{i=1}^{k} X_{\text{dissolved},i}, \quad \text{and}$$

$$X_{\text{insoluble}} = \sum_{i=1}^{k} X_{\text{insoluble},i} \tag{9}$$

If no absorption or luminal degradation occurs, mass-balance requires

$$X_{\text{solid}} + X_{\text{dissolved}} + X_{\text{insoluble}} \stackrel{!}{=} X_0 \tag{10}$$

at all times in the intestinal lumen. The concentration of dissolved drug is the relevant determinant of the simulation of the absorption process (see Fig. 1) as described in [24,26].

2.4. Experimental data used in this study

The data set of Jinno et al. [23] is ideally suited for the evaluation of the combined physiological dissolution and absorption model, because of the detail in experimental data that was

provided. The authors studied three different cilostazol suspensions with different particle size distributions: (a) hammer-milled crystal preparation with a median particle diameter of 13 μm, (b) a jet-milled cilostazol preparation with a median particle diameter of 2.4 μm, and (c) a cilostazol spray-dried powder (NanoCrystal® [56–58]) with a median particle diameter of 0.22 μm [23]. Further, the influence of both particle size and prandial state was investigated both *in vitro* and *in vivo*. Dissolution tests were performed in water as well as in biorelevant dissolution media reflecting the luminal contents of humans (fasted state simulating intestinal fluid (FaSSIF), and fed state simulating intestinal fluid (FeSSIF) [1,59,60]) at 37 °C using a USP Apparatus 2 DT-610 dissolution tester at 50 rpm [23]. Because the solubility of cilostazol was not high enough to dissolve the dose administered *in vivo* (100 mg) in 900 mL, the amount of cilostazol in the dissolution test was reduced 20-fold to 5 mg. The *in vivo* studies were carried out in beagle dogs with body weights between 8 and 10 kg (100 mg cilostazol per dog). Cilostazol plasma clearance was also determined from an additional study by the same authors with intravenous cilostazol administration and reported to be (5.4 ± 1.8) L/h (mean ± s.d.) [23]. Plasma concentration–time profiles after oral administration of the three suspensions under fasted and fed conditions were presented as well as the cumulative fraction dose absorbed, obtained after deconvolution of the oral data using the plasma profile following intravenous cilostazol administration.

The particle size distributions and *in vitro* dissolution profiles (mean values) as well as the *in vivo* plasma concentration–time profiles and cumulative fractions of the dose absorbed (mean and standard deviation) at a given time were obtained from the graphs shown in Ref. [23] after digitalization with a scanner using a read out software tool that was developed internally (ScanData, Bayer Technology Services GmbH, Leverkusen).

2.5. Pharmacokinetic simulations

All simulations were carried out using PK-Sim® Version 4.2 (Bayer Technology Services GmbH, Leverkusen). The physiological database of the software contains all species-specific physiological parameters of the beagle dog presented in Tables 1 and 2. The mathematical formalism for particle size-dependent dissolution and precipitation is an integral component of the software package in the form of an add-on dissolution module [61].

Basic physicochemical properties of the compound to be simulated, such as lipophilicity, fraction unbound in plasma, and molecular weight, are required for the simulations. These values were taken from public databases (Table 3) and used in PK-Sim® to calculate (i) the organ–plasma partition coefficients according to the model of Rodgers and Rowland described in [70] (see also Table 3) and (ii) the intestinal permeability coefficient of cilostazol. For the latter, a value of 3.4×10^{-4} cm/s was obtained using Eq. (9) and the parameter values listed in Table 1 of Ref. [26]. Furthermore, the cilostazol solubilities measured by Jinno et al. [23] in FaSSIF and FeSSIF were used to simulate fasted and fed conditions, respectively. Although the absorption model is also able to account for active influx and efflux processes, only passive absorption was taken into consideration for this study. This assumption is justified for cilostazol, since active transporters are reported to have only a minor influence on the absorption of this drug [62].

Table 3
Model parameters used and assumptions made for the PBPK simulations for cilostazol.

Parameter for cilostazol	Value	Comment, reference
Lipophilicity (Log *P*)	2.30	[68,69]
Fraction unbound in plasma	3.5%	[68,69]
Molecular weight	369.5 Dalton	[68,69]
Organ:plasma partition coefficients		[70]
–Bone	0.187	
–Brain	0.341	
–Fat	0.559	
–Gonads	0.127	
–Heart	0.288	
–Kidney	0.289	
–Large intestine	0.447	
–Liver	0.320	
–Lung	0.355	
–Muscle	0.166	
–Pancreas	0.380	
–Skin	0.544	
–Small intestine	0.447	
–Spleen	0.288	
–Stomach	0.447	
Body weight of beagle dog	9 kg	*In vivo* study: 8–10 kg [23] (default PK-Sim®: 10.5 kg [27])
Plasma clearance	(5.4 ± 1.8) L/h	Mean ± s.d. [23]
Intestinal permeability	3.4×10^{-4} cm/s	Calculated using Eq. (9) in [26]
Solubility (fasted state)	6.35 mg/L	Determined in FaSSIF [23]
Solubility (fed state)	12.7 mg/L	Determined in FeSSIF [23]
Particle size, geoMean (geoSD)		
–NanoCrystal formulation	0.25 μm (1.11)	See Fig. 2[a]
–Jet-Milled formulation	3.1 μm (1.43)	See Fig. 2[a]
–Hammer-Milled formulation	17.8 μm (1.73)	See Fig. 2[a]
Diffusion coefficient (*D*)	4.04×10^{-4} cm^2/min	[23]
Density (ρ)	1.26 g/cm^3	[23]
Thickness of the diffusion layer (h)	30 μm	[71]
Minimum particle radius (r_{min})	10 nm	See text
Treat precipitated drug as	Soluble	See text
Sink conditions?	Yes	See text

[a] As determined from the fit of the data from Jinno et al. to a log-normal particle size distribution function.

In the simulations, the dissolution kinetics were dynamically modeled during GI transit based on the Noyes–Whitney approach described above, using the measured solubilities of cilostazol in FaSSIF and FeSSIF. To this end, the particle size distribution had to be entered in the form of a mean value and standard deviation after selection of the appropriate distribution function (normal or log-normal distribution) in PK-Sim®. The density of the drug material and the diffusion coefficient of cilostazol were taken from Jinno et al. [23]. For all simulations, the apparent thickness of the diffusion layer was set to 30 μm in the model. This value was suggested by Heng et al. for nanoparticles of another BCS class II substance (cefuroxime axetil) [71]. The threshold for the minimal relevant particle radius was set to 10 nm based on an *a priori* estimate that the dissolution time for cilostazol particles of this size would be on the order of one minute and, thus, considerably smaller than the temporal resolution of our simulation (which was set to 10 points per hour, i.e., 6 min between consecutive time points). This estimate was confirmed by exemplary simulations demonstrating that a value of r_{min} = 10 nm yielded numerically identical results to simulations where r_{min} was set to 0.1 nm (which is below the diameter of a cilostazol molecule, data not shown). Because cilostazol is a neutral drug, precipitation in the model can only occur as a result of a decrease in the available volume of intestinal fluids. In the simulations, precipitation was assumed to be the inverse of the dissolution process according to scenario (a) in Fig. 1 that is described by Eq. (2), i.e., the precipitated amount was assumed to form a soluble cilostazol species rather than an insoluble form.

To visualize the impact of the observed inter-individual variability in the elimination of cilostazol, pharmacokinetic simulations were performed for the mean clearance (5.4 L/h) as well as for the mean plus and minus one standard deviation (i.e., 7.2 L/h and 3.6 L/h, respectively).

All simulations were carried out for a virtual male beagle dog with a body weight of 9 kg (the physiological parameters were scaled accordingly) assuming sink conditions in the whole GI tract. The resulting plasma concentration–time profiles under fasted and fed conditions for the three suspensions as well as the fractions dissolved and absorbed were compared with the data obtained experimentally by Jinno et al. [23]. A summary of the input parameters for the cilostazol simulations is presented in Table 3.

2.6. Parameter sensitivity analysis

In addition, a parameter sensitivity analysis was performed to analyze the effect of changes in the dissolution rate on the predicted maximum concentration and bioavailability. For this purpose, the dissolution parameter ζ_i that is inversely proportional to the particle radius (see Eq. (3)) was varied 1/4-, 1/2-, 2-, and 4-fold, relative to its default value. All other simulation parameters were kept constant, and the cilostazol plasma clearance was set to its mean value of 5.4 L/h [23].

3. Results

3.1. Cilostazol kinetics in dogs

The reported particle size distribution [23] could be best described by a log-normal distribution function (Fig. 2). The fitted median values were 0.23 μm, 2.9 μm, and 14.9 μm for the NanoCrystal®, jet-milled, and hammer-milled particles, respectively. These values were very similar to the reported median values (0.22 μm, 2.4 μm, and 13 μm [23], respectively). The fitted mean values and standard deviations of the log-normal distributions served as input parameters in the PK-Sim® dissolution module (Table 3).

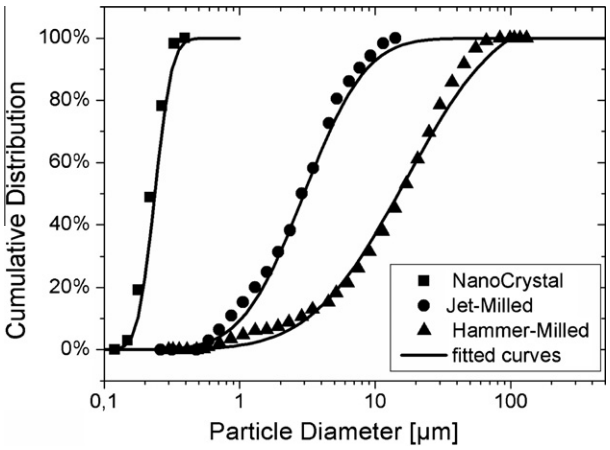

Fig. 2. Particle size distribution for the three cilostazol suspensions. Symbols represent the data from Ref. [23], the lines show the fit to a log-normal distribution function.

Fig. 3 shows the plasma concentration–time profiles of cilostazol predicted by the model (solid line) for the three types of suspensions in the fasted and fed state in comparison with the experimentally obtained data (symbols, mean, and s.d.). The gray-shaded area indicates the predicted range of plasma concentrations when the cilostazol plasma clearance is varied within one reported standard deviation. Fig. 4 summarizes mean predicted maximum plasma concentration (C_{max}) and bioavailability (F) in comparison with the experimental data (mean and s.d.). Bioavailability was calculated as the ratio of the simulated areas under the plasma concentration–time curves interpolated to infinity (AUC_{inf}) after oral administration and the mean AUC_{inf} after intravenous administration obtained in the study to allow better comparison with the experimentally obtained data.

Both figures demonstrate that the decrease in the rate and extent of absorption with increasing particle size is almost exactly predicted by the dynamic dissolution model.

Fig. 5 further elucidates the interplay of the dissolution and absorption rate as a function of particle size.

Here, the fraction dissolved in the GI tract (dotted lines) and fraction absorbed (solid lines) predicted by the model are shown together with the experimental *in vitro* dissolution data (open squares [23]) and the cumulated fraction absorbed obtained by a deconvolution of the *in vivo* plasma concentration–time profiles after oral and intravenous administration (closed symbols [23]). The dissolution profiles obtained *in vitro* by Jinno et al. deviate substantially from the simulated dissolution profiles during gastro-intestinal transit in the virtual dog and from the deconvoluted profiles. The overprediction of dissolution from *in vitro* experiments is likely a result of the application of sink conditions in those studies (which was done for practical reasons) and also resulted in overprediction of the *in vivo* plasma profiles (data not shown). By contrast, the time course of absorption predicted by combining the biorelevant solubilities, Noyes–Whitney description and PBPK simulation model is in excellent agreement with the *in vivo* data.

3.2. Parameter sensitivity analysis

The results of the parameter sensitivity analysis are summarized in Fig. 6. The sensitivity analysis demonstrates that an accurate determination of the dissolution parameter ζ_i is crucial for a successful prediction of the plasma kinetics of cilostazol. In the case of the hammer- and jet-milled suspensions, changing the particle size-dependent ζ_i by a factor of two leads to changes in C_{max} and F by a factor of 1.8 and 1.7, respectively. For the NanoCrystal®

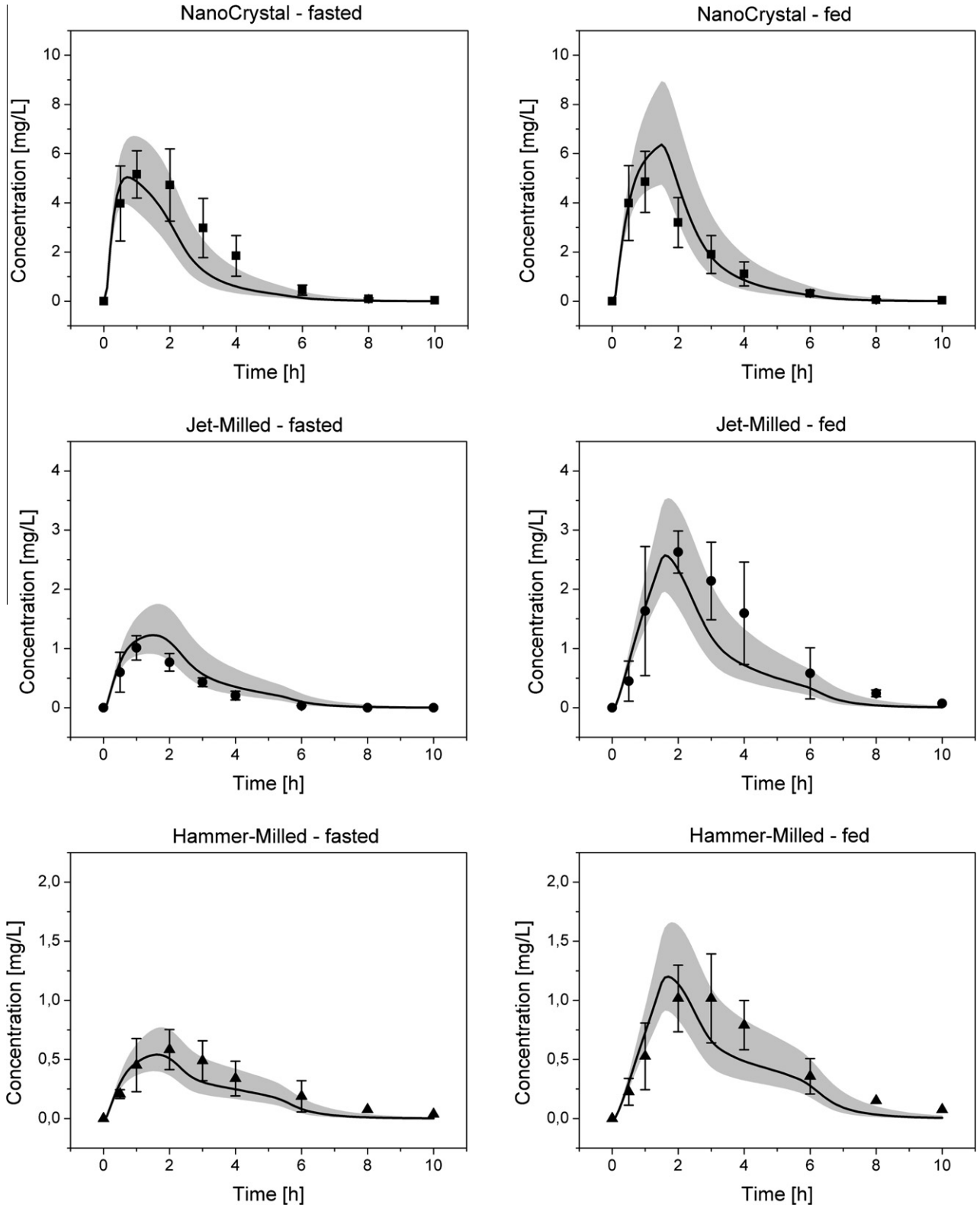

Fig. 3. Comparison of experimentally obtained plasma concentration–time profiles of the NanoCrystal (■), jet-milled (●), and hammer-milled (▲) suspensions in beagles (mean ± s.d. [23]) with the profiles simulated from the PBPK model. The solid lines represent the predictions from the particle size model for a mean cilostazol plasma clearance, and the gray-shaded area indicates the variability of the plasma concentrations due to the inter-individual clearance variability (standard deviations of the mean). The left column represents fasted conditions, the right column fed conditions.

formulation, the factors are 1.3 for C_{max} and 1.2 for F under fasted conditions, but only 1.1 for C_{max} and 1.0 for F under fed conditions, indicating lower sensitivity to particle size within the colloidal range.

4. Discussion

Physiologically based simulations of oral drug absorption are well established in the pharmaceutical industry [19,20] and have

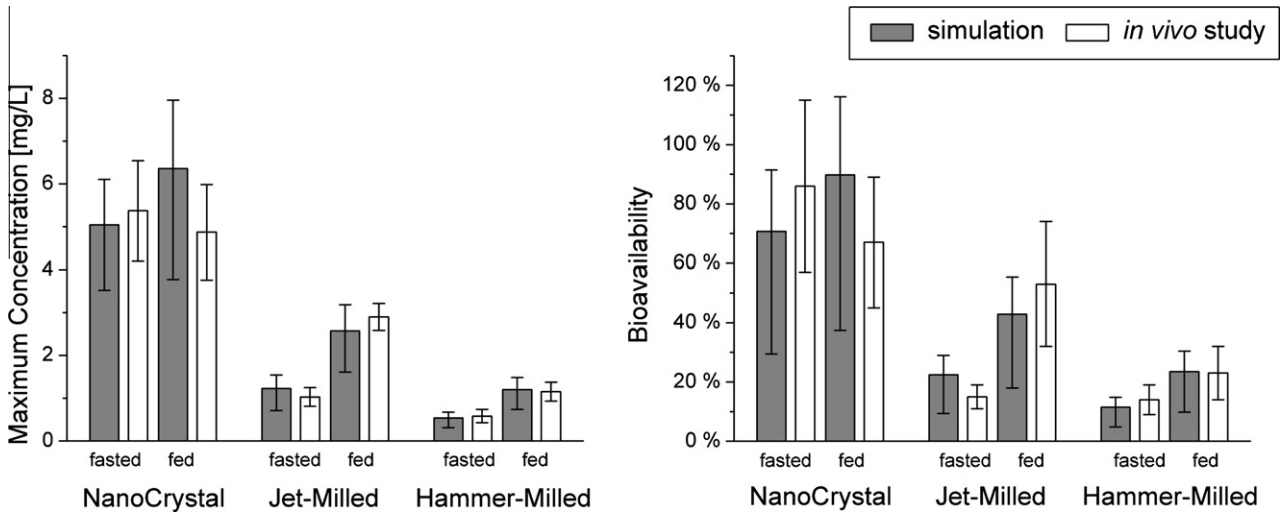

Fig. 4. Comparison of the maximum concentration and bioavailability predicted from the particle size with the experimentally obtained values (mean and s.d. [23]) of the three suspensions under fasted and fed conditions. The error bars represent the variability due to the inter-individual variability of the cilostazol clearance.

frequently been used in the past to streamline formulation development by designing formulation experiments [63], to interpret the outcome of *in vitro* dissolution and *in vivo* absorption studies [64–66], to predict food effects [17,67] and recently also to support biowaivers for BCS class 1 and 2 products [15,16,18]. Such models represent detailed physiological knowledge relevant for oral drug absorption with physico-chemical input information of the drug to be studied. In the present study, we added the information about gastro-intestinal physiology in beagle dogs (Table 1) to a previously established PBPK model for oral drug absorption [24–26] and combined it with a mathematical formalism that describes the dissolution process in dependence of the particle size, diffusion coefficient, density of the drug material, and intestinal solubility [55] in order to predict the influence of particle size on the plasma pharmacokinetics of cilostazol in beagle dogs.

Cilostazol was chosen as a model drug because of the availability of a rich experimental data set consisting of *in vitro* solubility and dissolution data in biorelevant media (FaSSIF and FeSSIF) and *in vivo* data obtained in fasted and fed beagle dogs for three different suspensions containing drug particles with different particle sizes [23]. This study thus provided a unique data set with respect to the influence of particle size on the rate and extent of *in vitro* and *in vivo* dissolution. The predictability of the *in vivo* outcome suffered from the fact that the dose in the *in vitro* dissolution test was chosen to be 20-fold lower (5 mg cilostazol) than the dose administered in the *in vivo* study (100 mg per dog) [23]. It was therefore to be expected that dissolution occurs at a much faster rate in the *in vitro* setting than *in vivo* in the dogs. Consequently, a quantitative IVIVC was not achieved by the authors [23]. But this gap could be fully closed with the application of the mechanistic dissolution and absorption model. Based on parameters that were derived from solubility data in biorelevant media and particle size data and taking into account decreasing particle size with ongoing dissolution, the combined dissolution and PBPK model was able to correctly translate the *in vitro* situation into the *in vivo* situation. The plasma concentration–time profiles observed in dogs under both fasted and fed conditions could be very well described by this model (Fig. 3). In particular, the lower maximum plasma concentration and bioavailability in case of the jet-milled and hammer-milled particles in comparison with the NanoCrystal® formulation was accurately predicted based on the *in vitro* solubilities in FaSSIF and FeSSIF (Fig. 4). This finding underscores the relevance of obtaining solubility and dissolution results in biorelevant media rather than in an aqueous buffer system.

The model predicted a positive food effect for all cilostazol suspensions, i.e., a trend towards higher C_{max} values and bioavailabilities in the fed state compared to the fasted state. This concurred with *in vivo* data for the hammer-milled and jet-milled suspensions, but not for the NanoCrystal® preparation. The latter exhibited a slightly negative (but insignificant) food effect [23] that was explained in the paper by a potential adsorption of the drug to ingested food. Interestingly, the PBPK model predicts that about 10% precipitation would occur in the small intestine of a fasted beagle for the NanoCrystal® suspension, as can be seen by the decreasing fraction dissolved over time, starting two hours after administration (Fig. 5). The timing of the predicted precipitation corresponds to arrival of the dose in the lower ileum, where supersaturation results from the lower volume of fluid available. As the simulation does not predict precipitation in the fed state, this might explain the prediction of a positive food effect by the model. On the other hand, the simulations also suggest that this finding might have been caused by the large inter-individual variability of the cilostazol clearance. Jinno et al. determined cilostazol plasma clearance in a second group of beagles ($N = 4$) and found a 30% coefficient of variation. When this large inter-individual variability in the elimination of cilostazol is considered, the slightly positive food effect predicted for the NanoCrystal® suspension becomes insignificant (gray-shaded areas in Fig. 3, error bars in Fig. 4).

As expected from the good agreement between the predicted and observed plasma concentration–time profiles, the predicted time courses of absorption also closely match the observed profiles. In case of the hammer-milled and jet-milled suspensions, the model correctly predicts that dissolution is the rate-limiting step for absorption, while permeation across the intestinal epithelium is identified as the rate-limiting step for absorption in the case of the NanoCrystal® formulation in both fasted and fed states. A correct identification of the rate-limiting step requires a precise value for the dissolution parameter ζ_i, and, thus, of the particle size, particle density, diffusion coefficient, and diffusion layer thickness. The latter was set to a constant value 30 μm irrespective of the particle size [71]. Although theoretical considerations postulate that the diffusion layer thickness should be similar to the particle size for particles that are smaller than approximately 20–30 μm [72], there are experimental findings that indicate a much larger apparent diffusion layer thickness (yielding to a lower rate of dissolution) in particular for BCS class II compounds. In one case, cefuroxime axetil nanoparticles exhibited an apparent diffusion

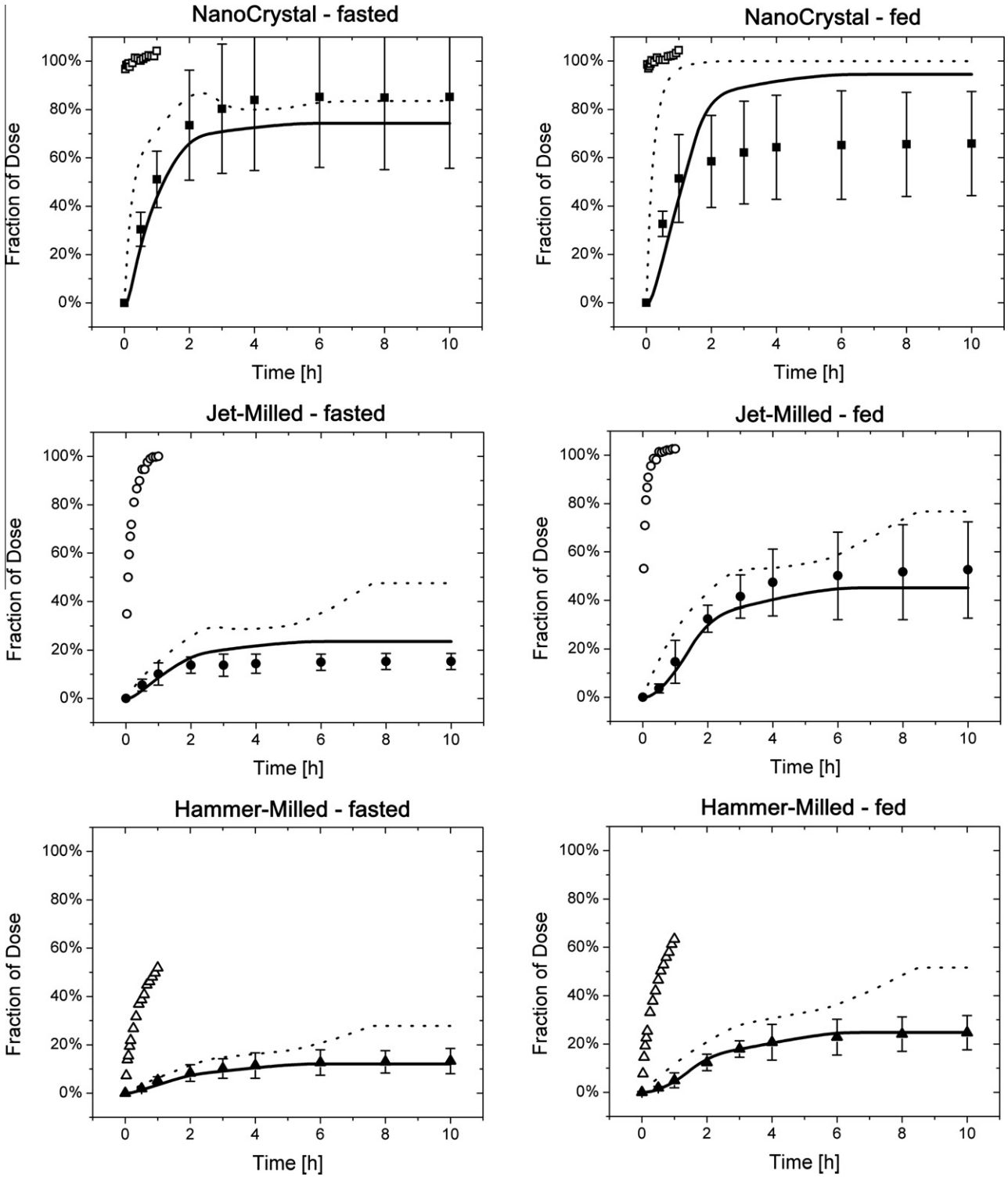

Fig. 5. Time courses of drug dissolution and absorption predicted from the particle size-dependent dissolution model in comparison with experimental data. Open symbols represent the *in vitro* dissolution data (mean ± s.d. [23]), closed symbols the *in vivo* fraction dose absorbed obtained by deconvolution of the plasma profiles after oral and intravenous administration (mean ± s.d. [23]). Dashed lines show the dissolution–time profile and solid lines the fraction dose absorbed predicted by the model for the NanoCrystal, jet-milled, and hammer-milled suspensions in the fasted (left column) and fed state (right column).

layer thickness of 30 μm that has been explained by aggregation phenomena [71]. In another example, Parrott et al. [73] reported a 21-fold overestimation of the dissolution parameter of aprepitant, when the diffusion layer thickness was set to the initial value of the particle size (5 μm in this example).

Overall, the sensitivity analysis demonstrated that uncertainty of ζ_i within a factor of two already drastically influences the quality of prediction, in particular in case of the dissolution-limited scenarios. Thus, a good estimate of the parameters essential to dissolution is crucial for a reliable prediction using this mechanistic

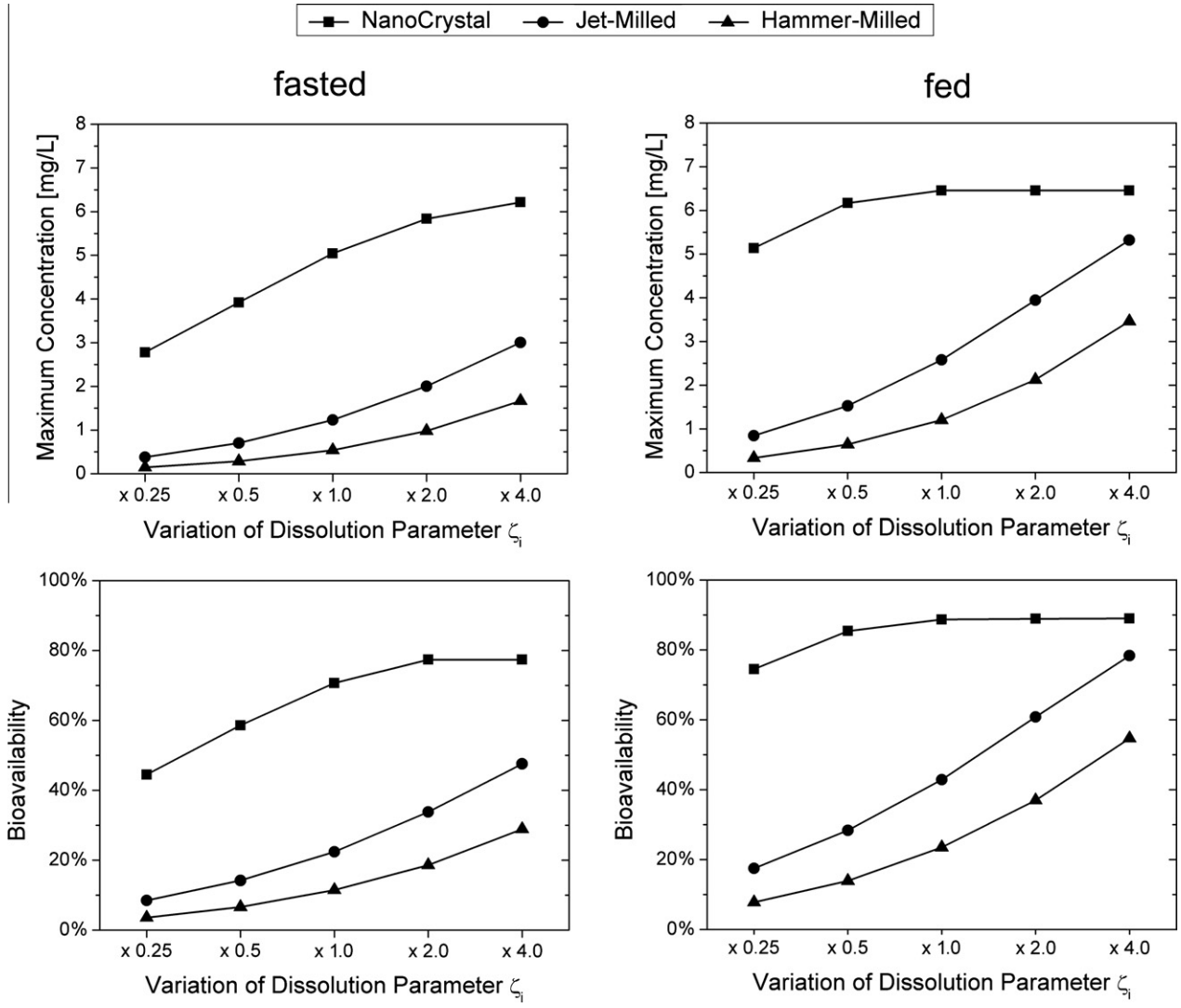

Fig. 6. Analysis of the sensitivity of maximum plasma concentration and bioavailability predicted by the particle size model with respect to changes in the dissolution parameter ζ_i in the fasted (left column) and fed state (right column).

PBPK model. Furthermore, the sensitivity analysis indicates what particle size reduction will be necessary in order to shift the rate-limiting step from dissolution (i.e. formulation related) to permeability (drug related), which is of particular relevance in the context of formulation optimization.

5. Conclusions

In conclusion, a mechanistic model that simulates the dissolution of a solid dosage form during gastro-intestinal transit in dependence of the particle size of the drug material under physiological conditions was developed. The model correctly predicted the influence of particle size on the rate and extent of cilostazol absorption in beagle dogs under fasted and fed conditions and was able to bridge the gap between the *in vitro* dissolution test results and the outcome of the *in vivo* study. Application of the PBPK model to formulation development should aid in the selection of an appropriate drug particle size in solid oral dosage forms.

References

[1] E. Galia, E. Nicolaides, D. Horter, R. Lobenberg, C. Reppas, J.B. Dressman, Evaluation of various dissolution media for predicting in vivo performance of class I and II drugs, Pharm. Res. 15 (1998) 698–705.

[2] E. Jantratid, M. De, V.E. Ronda, V. Mattavelli, M. Vertzoni, J.B. Dressman, Application of biorelevant dissolution tests to the prediction of in vivo performance of diclofenac sodium from an oral modified-release pellet dosage form, Eur. J. Pharm. Sci. 37 (2009) 434–441.

[3] E.S. Kostewicz, U. Brauns, R. Becker, J.B. Dressman, Forecasting the oral absorption behavior of poorly soluble weak bases using solubility and dissolution studies in biorelevant media, Pharm. Res. 19 (2002) 345–349.

[4] E. Nicolaides, E. Galia, C. Efthymiopoulos, J.B. Dressman, C. Reppas, Forecasting the in vivo performance of four low solubility drugs from their in vitro dissolution data, Pharm. Res. 16 (1999) 1876–1882.

[5] International Conference on Harmonisation Steering Committee, International Conference on Harmonisation of Technical Requirements for Registration of Pharmaceuticals for Human Use – Draft Consensus Guideline: Pharmaceutical Development Q8, 2004.

[6] The European Agency for the Evaluation of Medicinal Products (EMEA), Human Medicines Evaluation Unit, Committee for Proprietary Medicinal Products (CPMP), Note for Guidance on Development Pharmaceutics, 1998.

[7] The European Agency for the Evaluation of Medicinal Products (EMEA), Human Medicines Evaluation Unit, Committee for Proprietary Medicinal Products (CPMP), Note for Guidance on Modified Release Oral and Transdermal Dosage Forms: Section II (Pharmacokinetic and Clinical Evaluation), 1999.

[8] US Department of Health and Human Services, Food and Drug Administration, Center for Drug Evaluation and Research (CDER), Extended Release Oral Dosage Forms: Development, Evaluation, and Application of In Vitro/In Vivo Correlations (Guidance for Industry), US Government Printing Office, 1997.

[9] US Department of Health and Human Services, Food and Drug Administration, Center for Drug Evaluation and Research (CDER), Nonsterile Semisolid Dosage Forms; Scale-Up and Post-Approval Changes: Chemistry, Manufacturing, and Controls; In-Vitro Release Testing and In-Vivo Bioequivalence Documentation (Guidance for Industry), US Government Printing Office, 1997.

[10] G.L. Amidon, H. Lennernas, V.P. Shah, J.R. Crison, A theoretical basis for a biopharmaceutic drug classification: the correlation of in vitro drug product dissolution and in vivo bioavailability, Pharm. Res. 12 (1995) 413–420.
[11] The European Agency for the Evaluation of Medicinal Products (EMEA), Human Medicines Evaluation Unit, Committee for Proprietary Medicinal Products (CPMP), Note for Guidance on the Investigation of Bioavailability and Bioequivalence, 2001.
[12] US Department of Health and Human Services, Food and Drug Administration, Center for Drug Evaluation and Research (CDER), Waiver of In Vivo Bioavailability and Bioequivalence Studies for Immediate-Release Solid Oral Dosage Forms Based on a Biopharmaceutics Classification System (Guidance for Industry), 2000.
[13] World Health Organization, WHO Expert Committee on Specifications for Pharmaceutical Preparations – WHO Technical Report Series, No. 937: 40th Report, 2006.
[14] I. Kovacevic, J. Parojcic, I. Homsek, M. Tubic-Grozdanis, P. Langguth, Justification of biowaiver for carbamazepine, a low soluble high permeable compound, in solid dosage forms based on IVIVC and gastrointestinal simulation, Mol. Pharm. 6 (2009) 40–47.
[15] I. Kovacevic, J. Parojci, M. Tubi-Grozdanis, P. Langguth, An investigation into the importance of "very rapid dissolution" criteria for drug bioequivalence demonstration using gastrointestinal simulation technology, AAPS J. 11 (2009) 381–384.
[16] A. Okumu, M. DiMaso, R. Lobenberg, Computer simulations using GastroPlus to justify a biowaiver for etoricoxib solid oral drug products, Eur. J. Pharm. Biopharm. 72 (2009) 91–98.
[17] Y. Shono, E. Jantratid, N. Janssen, F. Kesisoglou, Y. Mao, M. Vertzoni, C. Reppas, J.B. Dressman, Prediction of food effects on the absorption of celecoxib based on biorelevant dissolution testing coupled with physiologically based pharmacokinetic modeling, Eur. J. Pharm. Biopharm. 73 (2009) 107–114.
[18] M. Tubic-Grozdanis, M.B. Bolger, P. Langguth, Application of gastrointestinal simulation for extensions for biowaivers of highly permeable compounds, AAPS J. 10 (2008) 213–226.
[19] J.B. Dressman, K. Thelen, E. Jantratid, Towards quantitative prediction of oral drug absorption, Clin. Pharmacokinet. 47 (2008) 655–667.
[20] K. Sugano, Introduction to computational oral absorption simulation, Expert Opin. Drug Metab. Toxicol. 5 (2009) 259–293.
[21] SimulationsPlus I. Simulations *plus*, Inc. Integrating Science and Software, 2009. <http://www.simulations-plus.com/Publication.aspx?pID=11> (accessed 1.10.09).
[22] Bayer Technology Services GmbH. Computational Systems Biology – Services and Solutions by Bayer Technology Services, 2009. <http://www.systems-biology.com/refs/pubs.html> (accessed 1.10.09).
[23] J. Jinno, N. Kamada, M. Miyake, K. Yamada, T. Mukai, M. Odomi, H. Toguchi, G.G. Liversidge, K. Higaki, T. Kimura, Effect of particle size reduction on dissolution and oral absorption of a poorly water-soluble drug, cilostazol, in beagle dogs, J. Controlled Release 111 (2006) 56–64.
[24] S. Willmann, W. Schmitt, J. Keldenich, J.B. Dressman, A physiologic model for simulating gastrointestinal flow and drug absorption in rats, Pharm. Res. 20 (2003) 1766–1771.
[25] S. Willmann, A.N. Edginton, J.B. Dressman, Development and validation of a physiology-based model for the prediction of oral absorption in monkeys, Pharm. Res. 24 (2007) 1275–1282.
[26] S. Willmann, W. Schmitt, J. Keldenich, J. Lippert, J.B. Dressman, A physiological model for the estimation of the fraction dose absorbed in humans, J. Med. Chem. 47 (2004) 4022–4031.
[27] A.C. Andersen, The Beagle as an Experimental Dog, Iowa University Press, Ames, Iowa, 1970.
[28] T.T. Kararli, Comparison of the gastrointestinal anatomy, physiology, and biochemistry of humans and commonly used laboratory animals, Biopharm. Drug Dispos. 16 (1995) 351–380.
[29] D.B. Paulsen, K.K. Buddington, R.K. Buddington, Dimensions and histologic characteristics of the small intestine of dogs during postnatal development, Am. J. Vet. Res. 64 (2003) 618–626.
[30] M.E. Miller, H.E. Evans, Millefs Anatomy of the Dog, Saunders, Philadelphia, 1979.
[31] F. Vaxman, A. Lambert, J.F. Grenier, Small bowel biopsy by remote control: experimental study on dogs, Dig. Dis. Sci. 41 (1996) 295–300.
[32] K.N. Kuzmuk, K.S. Swanson, K.A. Tappenden, L.B. Schook, G.C. Fahey Jr., Diet and age affect intestinal morphology and large bowel fermentative end-product concentrations in senior and young adult dogs, J. Nutr. 135 (2005) 1940–1945.
[33] A.B. Taylor, J.H. Anderson, Scanning electron microscope observations of mammalian intestinal villi, intervillus floor and crypt tubules, Micron 3 (1972) 430–453.
[34] J.H. Anderson, A.B. Taylor, Scanning and transmission electron microscopic studies of jejunal microvilli of the rat, hamster and dog, J. Morphol. 141 (1973) 281–291.
[35] J.B. Dressman, Comparison of canine and human gastrointestinal physiology, Pharm. Res. 3 (1986) 123–131.
[36] N. Katori, N. Aoyagi, S. Kojima, Effects of atropine and loperamide on the agitating force and GI transit time in dogs in drug absorption studies, Biol. Pharm. Bull. 19 (1996) 1338–1340.
[37] N. Katori, N. Aoyagi, S. Kojima, Effects of codeine on the agitating force and gastrointestinal transit time in dogs, for use in drug absorption studies, Biol. Pharm. Bull. 21 (1998) 418–420.
[38] H. Mizuta, Y. Kawazoe, K. Ogawa, Effect of small intestinal transit time on gastrointestinal absorption of 2-[3-(3,5-di-tert-butyl-4-hydroxyphenyl)-1H-pyrazolo[3,4-b]pyridin-1-yl] ethyl acetate, a new non-steroidal anti-inflammatory agent, Chem. Pharm. Bull. (Tokyo) 38 (1990) 2825–2828.
[39] H. Mizuta, Y. Kawazoe, K. Ogawa, Gastrointestinal absorption of chlorothiazide: evaluation of a method using salicylazosulfapyridine and acetaminophen as the marker compounds for determination of the gastrointestinal transit time in the dog, Chem. Pharm. Bull. (Tokyo) 38 (1990) 2810–2813.
[40] K. Sagara, Y. Nagamatsu, I. Yamada, M. Kawata, H. Mizuta, K. Ogawa, Bioavailability study of commercial sustained-release preparations of diclofenac sodium in gastrointestinal physiology regulated-dogs, Chem. Pharm. Bull. (Tokyo) 40 (1992) 3303–3306.
[41] K. Sagara, H. Mizuta, M. Ohshiko, M. Shibata, K. Haga, Relationship between the phasic period of interdigestive migrating contraction and the systemic bioavailability of acetaminophen in dogs, Pharm. Res. 12 (1995) 594–598.
[42] T. Itoh, T. Higuchi, C.R. Gardner, L. Caldwell, Effect of particle size and food on gastric residence time of non-disintegrating solids in beagle dogs, J. Pharm. Pharmacol. 38 (1986) 801–806.
[43] T. Miyabayashi, J.P. Morgan, M.A.O. Atilola, L. Muhumuza, Small intestinal emptying time in normal beagle dogs, Vet. Radiol. 27 (1986) 164–168.
[44] H. Mizuta, Y. Kawazoe, K. Haga, K. Ogawa, Effects of meals on gastric emptying and small intestinal transit times of a suspension in the beagle dog assessed using acetaminophen and salicylazosulfapyridine as markers, Chem. Pharm. Bull. (Tokyo) 38 (1990) 2224–2227.
[45] M. Smeets-Peeters, T. Watson, M. Minekus, R. Havenaar, A review of the physiology of the canine digestive tract related to the development of in vitro systems, Nutr. Res. Rev. 11 (1998) 45–69.
[46] C.Y. Lui, G.L. Amidon, R.R. Berardi, D. Fleisher, C. Youngberg, J.B. Dressman, Comparison of gastrointestinal pH in dogs and humans: implications on the use of the beagle dog as a model for oral absorption in humans, J. Pharm. Sci. 75 (1986) 271–274.
[47] H.W. Smith, Observations on the flora of the alimentary tract of animals and factors affecting its composition, J. Pathol. Bacteriol. 89 (1965) 95–122.
[48] C.A. Youngberg, J. Wlodyga, S. Schmaltz, J.B. Dressman, Radiotelemetric determination of gastrointestinal pH in four healthy beagles, Am. J. Vet. Res. 46 (1985) 1516–1521.
[49] D. Pinkel, The use of body surface area as a criterion of drug dosage in cancer chemotherapy, Cancer Res. 18 (1958) 853–856.
[50] US Department of Health and Human Services, Food and Drug Administration, Center for Drug Evaluation and Research (CDER), Center for Biologics Evaluation and Research (CBER), Estimating the Safe Starting Dose in Clinical Trials for Therapeutics in Adult Healthy Volunteers (Guidance for Industry and Reviewers), 2002.
[51] R. Kawai, M. Lemaire, J.L. Steimer, A. Bruelisauer, W. Niederberger, M. Rowland, Physiologically based pharmacokinetic study on a cyclosporin derivative, SDZ IMM 125, J. Pharmacokinet. Biopharm. 22 (1994) 327–365.
[52] H. Adachi, W. Strauss, H. Ochi, H.N. Wagner Jr., The effect of hypoxia on the regional distribution of cardiac output in the dog, Circ. Res. 39 (1976) 314–319.
[53] B. Davies, T. Morris, Physiological parameters in laboratory animals and humans, Pharm. Res. 10 (1993) 1093–1095.
[54] E.W. Quillen Jr., I.A. Reid, Effect of intravertebral angiotensin II on cardiac output and its distribution in conscious dogs, Circ. Res. 63 (1988) 702–711.
[55] K.C. Johnson, Dissolution and absorption modeling: model expansion to simulate the effects of precipitation, water absorption, longitudinally changing intestinal permeability, and controlled release on drug absorption, Drug Dev. Ind. Pharm. 29 (2003) 833–842.
[56] G.G. Liversidge, K.C. Cundy, Particle size reduction for improvement of oral bioavailability of hydrophobic drugs: I. Absolute oral bioavailability of nanocrystalline danazol in beagle dogs, Int. J. Pharm. 125 (1995) 91–97.
[57] E. Merisko-Liversidge, G.G. Liversidge, E.R. Cooper, Nanosizing: a formulation approach for poorly-water-soluble compounds, Eur. J. Pharm. Sci. 18 (2003) 113–120.
[58] Y. Wu, A. Loper, E. Landis, L. Hettrick, L. Novak, K. Lynn, C. Chen, K. Thompson, R. Higgins, U. Batra, et al., The role of biopharmaceutics in the development of a clinical nanoparticle formulation of MK-0869: a Beagle dog model predicts improved bioavailability and diminished food effect on absorption in human, Int. J. Pharm. 285 (2004) 135–146.
[59] J.B. Dressman, G.L. Amidon, C. Reppas, V.P. Shah, Dissolution testing as a prognostic tool for oral drug absorption: immediate release dosage forms, Pharm. Res. 15 (1998) 11–22.
[60] E. Jantratid, N. Janssen, C. Reppas, J.B. Dressman, Dissolution media simulating conditions in the proximal human gastrointestinal tract: an update, Pharm. Res. 25 (2008) 1663–1676.
[61] Bayer Technology Services GmbH, PK-Sim User Manual and Software, 4.1, 2009.
[62] H. Toyobuku, I. Tamai, K. Ueno, A. Tsuji, Limited influence of P-glycoprotein on small-intestinal absorption of cilostazol, a high absorptive permeability drug, J. Pharm. Sci. 92 (2003) 2249–2259.
[63] M. Kuentz, S. Nick, N. Parrott, D. Rothlisberger, A strategy for preclinical formulation development using GastroPlus as pharmacokinetic simulation tool and a statistical screening design applied to a dog study, Eur. J. Pharm. Sci. 27 (2006) 91–99.

[64] V. Lukacova, W.S. Woltosz, M.B. Bolger, Prediction of modified release pharmacokinetics and pharmacodynamics from in vitro, immediate release, and intravenous data, AAPS J. 11 (2009) 323–334.
[65] A. Okumu, M. DiMaso, R. Lobenberg, Dynamic dissolution testing to establish in vitro/in vivo correlations for montelukast sodium, a poorly soluble drug, Pharm. Res. 25 (2008) 2778–2785.
[66] K. Thelen, E. Jantratid, J.B. Dressman, J. Lippert, S. Willmann, Analysis of nifedipine absorption from soft gelatin capsules using PBPK modeling and biorelevant dissolution testing, J. Pharm. Sci. 99 (2010) 2899–2904.
[67] N. Parrott, V. Lukacova, G. Fraczkiewicz, M.B. Bolger, Predicting pharmacokinetics of drugs using physiologically based modeling – application to food effects, AAPS J. 11 (2009) 45–53.
[68] D.S. Wishart, C. Knox, A.C. Guo, S. Shrivastava, M. Hassanali, P. Stothard, Z. Chang, J. Woolsey, DrugBank: a comprehensive resource for in silico drug discovery and exploration, Nucleic Acids Res. 34 (2006) 668–672.
[69] D.S. Wishart, C. Knox, A.C. Guo, D. Cheng, S. Shrivastava, D. Tzur, B. Gautam, M. Hassanali, DrugBank: a knowledgebase for drugs, drug actions and drug targets, Nucleic Acids Res. 36 (2008) 901–906.
[70] T. Rodgers, M. Rowland, Physiologically based pharmacokinetic modelling 2: predicting the tissue distribution of acids, very weak bases, neutrals and zwitterions, J. Pharm. Sci. 95 (2006) 1238–1257.
[71] D. Heng, D.J. Cutler, H.-K. Chan, J. Yun, J.A. Rap, Dissolution kinetic behavior of drug nanoparticles and their conformity to the diffusion model, Langmuir 24 (2008) 7538–7544.
[72] K. Sugano, Theoretical comparison of hydrodynamic diffusion layer models used for dissolution simulation in drug discovery and development, Int. J. Pharm. 363 (2008) 73–77.
[73] N. Parrott, V. Lukacova, G. Fraczkiewicz, M.B. Bolger, Predicting pharmacokinetics of drugs using physiologically based modeling—application to food effects, AAPS J. 11 (2009) 45–53.